Mechanical Properties and Microstructure Analysis of Mild Steel Welding Made by GTAW

Saleh Suliman Saleh Elfallah[*]
College of Mechanical Engineering Technology, Benghazi, LIBYA
[*]*sselfallah87@email.com*

ABSTRACT

This work discusses the effect of gas tungsten arc welding (GTAW) variables on the welding transverse tensile strength and hardness of S 235JR at different groove configurations. The welding microstructure and numerical fracture mechanism are also discussed. GTAW is increasingly emerging in the local industry due to its advantages over conventional shielded metal arc welding (SMAW). The properties of steel welding have always concerned manufacturers and researchers. Since steel structures experience forces such as tensile, it's vital that good welding has increased tensile strength. It was reported that the hardness of welding affects the welding properties and, therefore, the integration of welded structures. The groove shape of the joining ends determines the size of the FZ and affects the dilution; thus, it is important to study the groove shape due to its effect on the final properties of welding. The results showed an increased welding traverse tensile strength (251 MPa) at higher welding speeds (150 mm/min) and V-shaped groove welding. The V-shaped groove welding that obtained higher tensile strength (251 MPa) has shown higher grain boundary ferrite and PF volume friction in the FZ and finer PF in the HAZ due to its higher interpass heat input. Higher traverse tensile strength welding has shown increased bainite and lower bainite volume friction in FZ and a finer grain structure in HAZ. The failure due to tensile force starts at the welding root, according to numerical analysis, and a double V-shaped groove has shown deformation balance at the tensile test.

Keywords: *GTAW; Mild Steel; Mechanical Properties; Microstructure, Numerical Fracture Mechanism*

ISSN 1823-5514, eISSN 2550-164X

https://doi.org/10.24191/jmeche.v21i3.27361

Received for review: 2024-01-03
Accepted for publication: 2024-05-27
Published: 2024-09-15

Introduction

Gas tungsten arc welding (GTAW) is a common welding process utilized in industry due to its high quality, low energy consumption, and sustainable environment [1]. It also has higher welding penetration [2], and it is commonly used for thinner base metal sheets [3]. GTAW uses a non-consumable zirconated electrode along with protective shielding gas [4]. A filler material is usable to fill large joint gaps in thick base metal [5]. GTAW has been widely used to weld dissimilar metals such as carbon steel with stainless steel [2], Inconel with stainless steel [6], and ferritic with martensitic of P 92 steel grade [7]. It was reported that GTAW is commonly used to weld aluminum alloys [8]. It has been tested on low-carbon steel as well [9]. Satheesh Kumar et al. [5] reported that GTAW has superior mechanical properties over GMAW for 316L stainless steel welding [5] and AISI 1045 steel welding [10].

Low-carbon steel, also referred to as mild steel or commercial steel, is vastly used in industry due to its excellent processing properties [11] and its various range of applications due to its excellent mechanical properties [12]. Different welding techniques, including shielded metal arc welding (SMAW), gas metal arc welding (GMAW), friction stir welding (FSW), and GTAW, have reported their ability to weld low-carbon steel [13]. GTAW is preferred over SMAW and GMAW due to its optimized welding cost and higher welding strength [10]. For its advantages, GTAW has been highly utilized in welding mild steel in the local industry in Benghazi, either in fabrication for hollow sections, structures, or sheets. However, the problem that always accompanies structural integrity is welding. Due to the difference in properties between the welding and base metal, such as the increased hardness of the heat-affected zone (HAZ) or the susceptibility of welding to cracking, it is prone to failure [10], [14]. A study by İrsel [15] on S235JR steel welding concluded that GTAW welding has superior strength and high-quality welding over SMAW, as well as smoother weld bead appearances.

It’s essential to optimize the welding settings for higher-quality welding with better mechanical performance. Welding variables such as welding current, welding voltage, welding speed, and gas flow rate have been studied by researchers to investigate their influence on the mechanical properties of welding, such as tensile strength and hardness [10]. There are multiple statistical and modelling approaches to optimizing the welding process, such as Taguchi’s design, full factorial design, fuzzy logic, general algorithm, neural network, and other techniques [10]. Studies have examined how welding variables affect GTAW welding's tensile strength. Abima et al. [4] studied the effect of welding variables on low carbon steel (AISI 1008) welding and found that welding current had a higher effect than shielding gas flow rate on the welding tensile strength. Another study on low-carbon steel welding by Mohanty et al. [12] using welding filler (ER309L) found that welding current had a higher effect on welding tensile strength and hardness.

In a previous study by Elfallah [16] on mild steel welding grade S235JR, tensile strength and hardness were shown at low welding currents. However, Korkmaz and Meran [1] concluded that increased welding current and welding speed showed higher tensile strength in the welding of XPF 800 steel. Abima et al. [4] reported similar increases in welding variables in low-carbon steel welding, which led to an increase in welding tensile strength and a decrease in hardness. Jawad et al. [10] reported that the tensile strength of medium steel AISI 1045 welding increased with increased welding current and decreased welding speed while the hardness decreased. A study by Luijan et al. [2] on the dissimilar welding of low carbon steel and 3 CR12 ferritic stainless steel resulted in higher welding hardness at higher welding current and welding speed, while the tensile strength showed an increase at 100 A and then a decrease at 130 A. The results also show that the hardness of the fusion zone (FZ) is lower than that of the HAZ, as also reported by Saidin et al. [14] on low-alloy steel welding, and that the hardness in general dropped at the transition between the FZ and HAZ. The latter has also been confirmed by Korkmaz and Meran [1]. These facts indicate that the hardness of welding, the FZ, and the HAZ interact with the tensile strength of the welding structure. It was reported that welding hardness affects other mechanical properties, such as in a study by Sirohi et al. [8] showing that higher welding hardness results in lower welding toughness.

The microstructure of welding was reported to influence the mechanical properties of welding. For instance, Sirohi et al. [7] reported that microstructure behaviour affects the hardness of welding P92 steel, i.e., the hardness decreased with increased homogeneity of welding microstructure. Durgaprasad et al. [9] concluded from a study on low-carbon steel welding that increased HAZ grain refinement has caused the hardness to increase. A similar result was obtained by Elfallah [16] in a study of S 235JR mild steel welding. However, the study showed that less developed grain structure, i.e., finer grains in HAZ and less pearlitic and widmanstatten ferrite in FZ, resulted in higher tensile strength in welding.

Despite the numerous researchers on the GTAW technique related to single-pass, relatively little research has been done on the effects of process parameters on the mechanical characteristics and FZ shape in GTAW. The groove shape was reported to affect the size of FZ and the mechanical properties of final welding [17]. Kant et al. [18] studied the effect of FZ geometry by ranging the V-shaped groove angle from 30° to 50° on the mechanical properties of IS:2062 mild steel. The study found that the welding current had a higher influence on the FZ width and the welding speed on the depth of penetration. The groove shape angle was found to be insignificant; however, higher tensile strength (406.2 MPa) was shown at the lower groove angle (30°). Dak et al. [19] concluded from a study on P 92/SS 304L dissimilar welding that a wider groove shape has increased residual stresses and lower toughness (33J) compared to 35J for narrower groove-shaped welding. Singh

et al. [17] also confirm that AISI 410 stainless steel welding with a smaller groove volume obtained maximum tensile strength (758.34 MPa) and maximum impact toughness (123.8 J). In contrast, Pathak et al. [20] reported on AISI 1016 low carbon steel welding that a higher groove shape angle (75°) has a higher hardness (122.1 HB). Çetkin et al. [21] worked on the welding of AA5182 and AA7075 aluminum alloys by varying groove shapes of V and double V-grooved shapes. The results concluded that maximum tensile strength (262.87 MPa) and hardness (89 VHN) were observed at double V-grooved shape welding. Furthermore, increased tensile strength and hardness were demonstrated for both groove shapes with increased welding current (150 A).

According to these studies, the welding current and welding voltage have a higher effect on the welding tensile strength and hardness than other common welding variables such as gas flow rate, groove shape, and other variables. Therefore, it's suggested in this study that the welding current be fixed to focus on this effect of other variables. The welding speed has been shown in the literature to have a significant effect on welding. Furthermore, the groove shape was included because it has been shown by previous studies to affect the properties of final welding. This study included the common V-shaped and double V-shaped groove configurations to investigate their impact on the mechanical properties, tensile strength, and hardness of the welding. Furthermore, numerical analysis was applied to demonstrate the welding fracture mechanism. This work tries to study how the welding speed with respect to the change in groove shape affects the final welding transverse tensile strength and hardness of S235JR mild steel and modelling the failure mechanism. The process was made using the GTAW technique and the common welding filler E6013. Besides, the welding microstructure behaviour of FZ and HAZ was discussed to determine their influences on that matter.

Methods and Materials

The base metal utilized for welding is mild steel. It follows the European standard EN 10025-2, grade S235JR (1.0038). The mild steel-grade E6013 welding filler used for welding is 2.5 mm in size. The material composition is shown in Table 1, and Table 2 shows their mechanical properties. The composition and properties of base metal and welding filler are based on test certificates EN10204-3.1 and AWS A5.1:E 6013, respectively. The Vickers microhardness in Table 2 is according to the standard hardness conversion ASTM E140-12B (2019)e1 [22] as a value converted from Brinell hardness 120 HB following the test certificate EN10204-3.1. However, the hardness conversion standard DIN EN ISO 18265 has recorded 126 VHN. The initial base metal was a 1000 mm by 800 mm sheet with a 10 mm thickness, cut into rectangular plates of 225 mm (450 mm after joining) by 50 mm. The base metal

grooves, V, and double V-shaped grooves were prepared using a JMTC electric bench grinder with water as a coolant at the College of Mechanical Engineering Technology in Benghazi. The welding process was controlled by the power supply, the Daewoo Inverter Welder GTAW/MMA, and the welding speed was controlled by the YSG-12 Beetle Portable Gas Cutter for controlled process speed, as shown in Figure 1. The welded samples are shown in Figure 2. Because the V-shaped groove has a wider groove gap than the double V-shaped groove, multiple passes were applied. After welding, the samples were prepared following the tensile test standard ASTM E8/E8M-22 [23], shaping the reduced section as illustrated in Figure 3. The process was made by a CNC laser cutter router, Senfeng®, in the Tasamim Workshop in Benghazi. Furthermore, other plates of 20 mm by 20 mm were welded (Figure 4) with the same settings and then sectioned by Remet® TR80 using coolant oil to be tested for hardness and inspected for microstructure.

Table 1: The chemical compositions of the base metal and welding filler for the welding process

Component	**Composition (%)**										
	C	**Mn**	**S**	**Ni**	**Cr**	**P**	**Si**	**Cu**	**Mo**	**V**	**Fe**
Base metal (S235JR)	0.17	1.4	0.025	0.012	-	0.025	-	0.55	-	-	Balance
Welding filler (E6013)	0.09	0.43	0.01	0.018	0.023	0.015	0.23	-	0.003	0.022	

Table 2: The tensile strength and hardness of base metal and welding filler

Component	**Tensile properties**		**Hardness properties**
	Yield strength (MPa)	**Tensile strength (MPa)**	**Vickers micro-hardness (VHN)**
Base metal (S235JR)	235	360-510	≈120 [22]
Welding filler (E6013)	442	510	-

A shielding gas made of 90% argon (Ar) and 10% carbon dioxide (CO_2) was applied in the welding process. CO_2 with 5% to 20% Ar has been widely utilized for welding mild steel due to the fact that argon alone causes arc instability and undesirable weld bead characteristics. While CO_2 has led to spattering issues [24]. Deepak et al. [25] reported the usage of an 80% to 20% Ar to CO_2 mixture shielding gas composition in the welding of low carbon steel. Purnama and Oktadinata [26] reported that shielding gas composed of a 90% Ar and 10% CO_2 mixture with filler metal has much fewer inclusions in weld metal than 100% CO_2. However, Murali and Gopi [27] reported that welding fabricated with 80% Ar and 20% CO_2 mixture shielding gas has a

higher tensile strength than welding made with 100% Ar. The gas flow rate is set to 10 ml/min. Table 3 lists the welding process setup variables of groove shape and welding speed, while the base metal thickness and welding current were fixed at 10 mm and 200 A, respectively. The welding voltage is estimated to be 30 V and decreases with time due to the power supply's reduced efficiency.

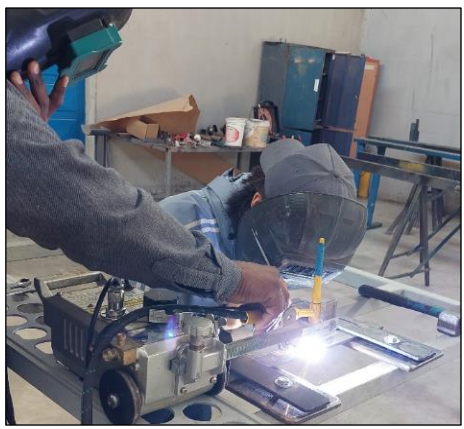

Figure 1: Welding process

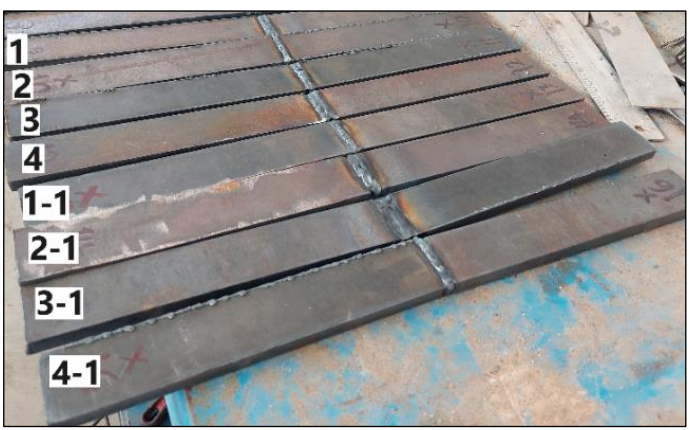

Figure 2: Welding samples welded at settings shown in Table 4

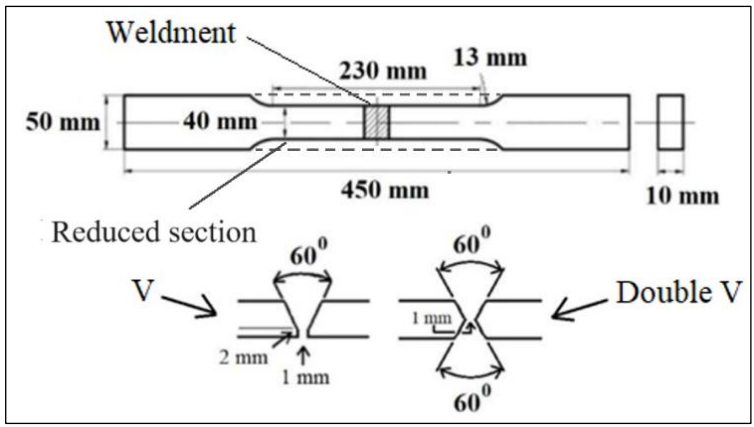

Figure 3: The dimensions of the samples for the tensile test were made in accordance with ASTM E8/E8M [23]

Figure 4: Welding samples for a hardness test and microstructure inspection

Table 3: Welding input variables

Factors	**Unit**	**Input 1**	**Input 2**
Welding speed	mm/min	100	150
Groove shape	-	V	Double V

The universal testing apparatus (Shimadzu (UEH-20)) at the Libyan Iron and Steel Company performed the tensile tests. Some of the tests were repeated by the sample's replicas due to the failure of the first tries. It's due to the failed samples breaking early and giving abnormal test results. Figure 5 displays the tensile-tested samples, all of which exhibit separation at the FZ and FZ/HAZ boundaries. As it will be discussed later, the variation in

mechanical properties such as hardness caused the separation; however, it's important to note that HAZ is naturally brittle and susceptible to failure [28].

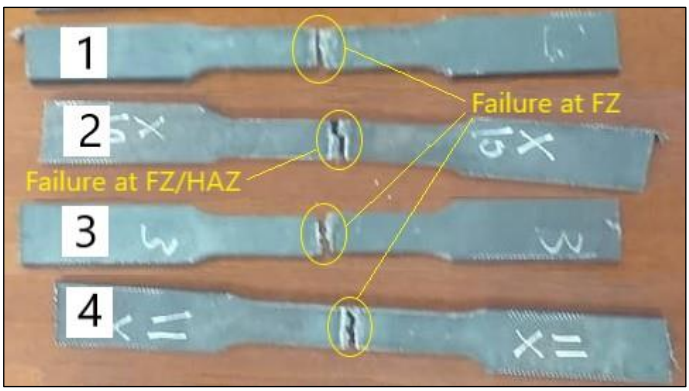

Figure 5: Tensile tested samples showing failure locations at FZ and FZ/HAZ

Table 4 lists the welding experiments with respect to the welding variation shown in Table 3. Table 4 also lists the tensile strength results as an average of two records, which correspond to two samples for every welding experiment. Bulut Makina Sanayi (BMS) micro-hardness testers from the High Vocational Center of Casting carried out the Vickers micro-hardness testing. The hardness was measured due to an indentation made by a diamond cone at 120° with a 1 kg force load pressed. The distribution of hardness positions on the sample cross-section is shown in Figure 6, and the results are shown in Figure 7. The hardness records listed in Table 4 are an average of hardness readings taken in FZ, HAZ, and base metal for each sample, as seen in Figures 6 and 7, which correspond to each welding experiment.

Table 4: Welding experiments with their corresponding tensile strength and Vickers micro-hardness results

Welding experiment no.	Welding speed (mm/min)	Groove shape	Tensile strength (N/mm^2)	Heat input (J/mm)	Vickers micro-hardness (VHN)		(N/mm^2) / VHN (FZ)	(N/mm^2) / VHN (HAZ)
					FZ	HAZ		
1	100	V	237	2160	267.8	277.5	0.88	0.85
2	100	Double V	212	2160	257.3	254.7	0.82	0.83
3	150	V	251	1440	268.6	275.0	0.93	0.91
4	150	Double V	228	1440	261.1	262.9	0.87	0.87

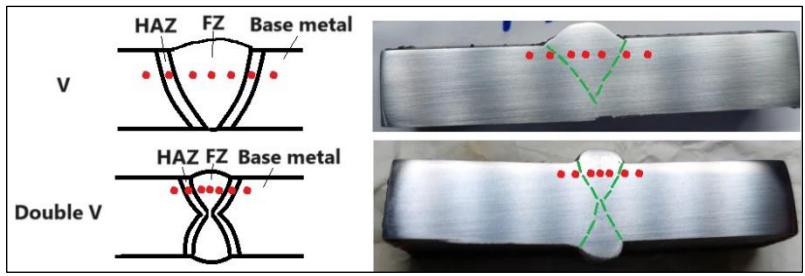

Figure 6: Distribution of the hardness test positions on the welding cross-section

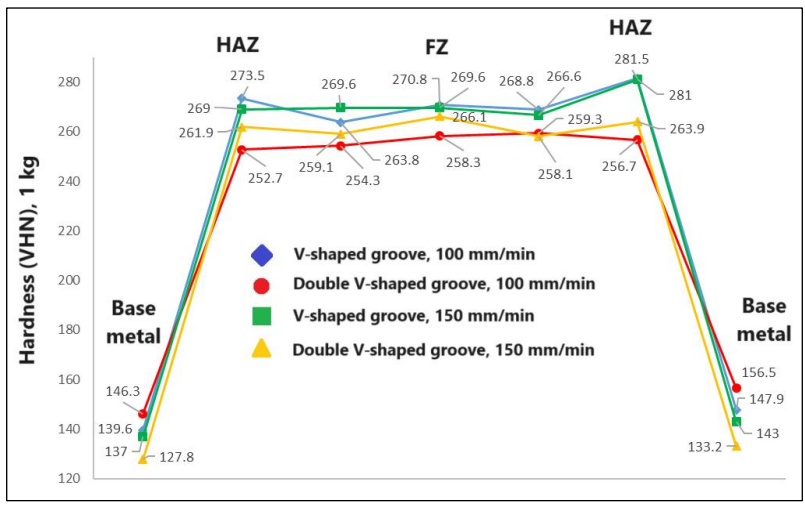

Figure 7: Hardness values in each region of the welding cross-section

The microstructure of samples was revealed by the Zeiss AxioCam ICC-5 optical microscope after being sectioned and grided with sandpapers from 80 grit to 1200 grit. The samples are polished with an aluminum oxide suspended power of 0.05 μm in grain size and etched by Nital for several seconds.

The finite element analysis (FEA) validation model was performed to replicate the failure result from the tensile test numerically by ABAQUS®. The effect of the welding groove shape is the sole factor determining the fracture differentiation mechanism between V and double V-shaped groove welding. However, such a model is not entirely precise because it didn't observe the dilution of welding, which may change to some extent the distribution of stresses at the welding. The finite element (FE) model is a full 3D model of

the tensile samples (Figure 3). The weld bead, or FZ, has chosen a geometry to fill in the groove, which consists of 121,400 hexahedral elements of type C3D8R with an 8-noded brick and 137,104 nodes.

Results and Discussion

This section discusses the effect of welding variables, such as welding speed and groove shape on the transverse tensile strength and hardness of welding and their microstructure behaviour. It also delved into the numerical fracturing mechanism that occurs at various groove shapes.

Effect of welding parameters on the mechanical properties

Table 5 shows that tensile strength has increased with increased welding speed and at the V-shaped groove. E.g., welding experiment number 3 showed a welding transverse tensile strength of 251 MPa at a welding speed of 150 mm/min, compared to experiment number 1 that showed 237 MPa at 100 mm/min. An average hardness of FZ has also increased with increased welding speed (e.g., the welding experiment number 3 obtained 268.6 VHN of FZ hardness at 150 mm/min, while the welding experiment number 1 had a FZ hardness of 267.8 VHN). However, HAZ's hardness has only increased at the double V-shaped groove. In general, HAZ has a higher hardness than FZ. It is more visible in Figure 7 for V-groove-shaped welding. In contrast, the base metal has shown a clearly lower hardness, with an average of 141.4 VHN. The decreased hardness of the base metal is attributed to the fact that it has not been affected by the welding heat input and has kept the original as-received properties of the heat-treated stock material. The lower hardness due to the microstructure's coarse grains is discussed below. A study by Voiculescu et al. [29] reported that the average base metal hardness of S235JR is 137 VHN when applied to a force load of 0.2 kg. While a study by Krella et al. [30] stated the base metal hardness is 148.5 VHN at 0.5 kg. The tensile strength-to-hardness ratio helps obtain visible hardness figures with respect to the corresponding tensile strength. It is noticeable that the hardness and tensile strength ratio (N/mm^2)/VHN were higher at FZ. E.g., the ratio at a V-shaped groove and 100 mm/min that corresponds to welding experiment number 1 was 0.88, that is, the tensile strength of welding (237 MPa) has 88% of an average FZ hardness value (267.8 VHN), compared to 85% of the hardness value of HAZ (277.5 VHN). The same pattern applies to all experiments except for welding experiment number 4, where the difference in hardness between the FZ and HAZ is close. It is interesting to note that the increased tensile strength-to-hardness ratio is associated with increased welding speed and reduced heat input. For example, in welding experiment 3, the ratio showed that the tensile strength (251 MPa) represented 93% and 91% of the FZ and HAZ hardness, respectively. In contrast to 88% and 85% at welding

experiment 1, both experiments were made in a V-shaped groove. A similar pattern occurred at the double V-shaped groove. However, a higher ratio at V-shaped groove welding over double V-shaped has shown higher tensile transverse welding strength (251 MPa at welding experiment 3 in contrast to 220 MPa at welding experiment 4). These results indicate that the increased welding hardness has contributed to higher welding tensile strength, and the smaller increment in hardness has resulted in a higher increment of tensile strength. This hypothesis is clear as the tensile strength-to-hardness ratio has increased. The failure in FZ or at the FZ/HAZ boundary could be related to the hardness variation; however, for more clarification, it's important to relate the results of microstructure and fracture numerical analysis.

The heat input (*HI*) of the welding process as shown in Table 4 is calculated from Equation (1), taking into consideration 0.6 as a thermal efficiency for GTAW [31]:

$$HI = \frac{\text{Voltage } (V) \times \text{Amperage } (A) \times 60}{\text{Travel speed (mm/min)}} \times 0.6 \quad (1)$$

The decreased heat input is associated with the increased welding speed since the welding current is fixed at 200 A and the voltage at 30 V. The heat input has reduced tensile strength and hardness. The increased heat input has been shown to cause a lower cooling rate, as reported by Scharf-Wildenhain et al. [32]. As a result, there are more internal residual stresses and strains in the FZ and HAZ. Research by Ji et al. [33] concluded that higher internal stresses result in lower hardness. Previous studies on mild steel welding by GTAW showed that lower hardness presented lower welding tensile strength [16]. Lahtinen et al. [34] on high-strength steel welding showed that lower strength was due to higher heat input, which caused early localization strain in the welding. The increased hardness at V-shaped groove welding could be related to the increased welding interpasses since the V-shaped groove has a deeper groove than the double V-shaped groove, as shown in Figure 3. It is reported by Scharf-Wildenhain et al. [32] that increased interpasses led to increased heat input between the passes. However, Sridharan et al. [35] mentioned that the interpass temperature plays a major role in controlling the residual stress evolution and reducing distortion.

Effect of welding parameters on the microstructure behaviour

The microstructure presented in Figure 8 is the base metal magnified 20 times as shown in Figure 8(a) and 100 times as shown in Figure 8(b). The base metal presents coarse α-ferrite (α) as light-contrast grains and large perlite (P) bands blended with carbide (i.e., iron carbide presented in darker contrast) mostly located in the middle of perlite grains. The perlite, as seen in Figure 8(b), appeared less dark than carbide due to the fact that it is a mixture of α-ferrite with cementite and is shown in clusters surrounding the carbide grains. In

general, the α-ferrite shown in wider areas than the perlite bands due to the mild steel having a carbon content of 0.17%. The base metal in Figure 8(a) also shows inclusions, which are mainly silicon, sulfur, or phosphorous concentrations and are reported to be the cause of welding embrittlement [36]. The higher the carbon content in steel, the more perlite there is, along with cemetite precipitation and reduced light-contrast grains of α-ferrite.

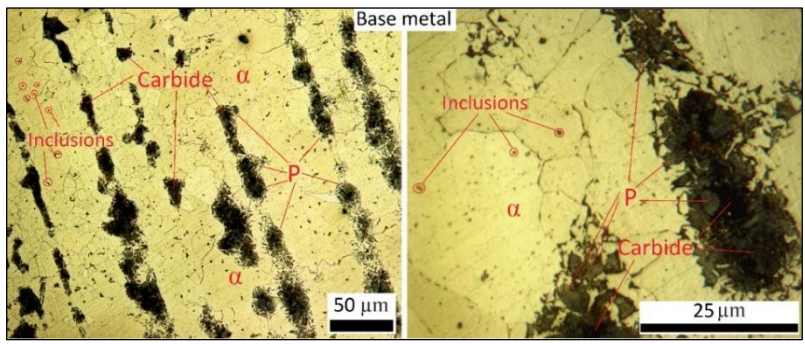

Figure 8: Base metal microstructure magnified; (a) 20 times, and (b) 100 times

The FZ microstructure for the welding experiments is shown in the optical view in Figure 9, magnified 20 times. The microstructure labelings a, b, c, and d correspond to welding experiments 1, 2, 3, and 4, respectively. The FZ microstructure in general showed the presence of acicular ferrite (AF), polygonal ferrite (PF), Widmanstätten ferrite (WF), bainite (B), lower bainite (LB), and grain boundary ferrite (GBF), which is also 'allotriomorphic ferrite' [37]. The FZ of welding experiment 1 (Figure 9(a)) presented to some extent an increased volume fraction of GBF than the FZ of welding experiment 3, as seen in Figure 9(c). The FZ of welding experiments 2 and 4 (Figures 9(b) and 9(d)) presented a lower GBF volume fraction and larger AF grains; however, they showed a higher volume fraction of B and LB. The welding experiment 1 (Figure 9(a)), which corresponds to V-shaped groove welding, was exposed to higher heat input as shown in Table 4, which led to FZ presenting an increased ferritic volume fraction (i.e., GBF, PF, and AF). However, welding experiment 2, which corresponds to double V-shaped groove welding, was also exposed to higher heat input but showed narrower ferritic grains. It is due to the fact that V-shaped groove welding had more welding interpasses that led to an increased temperature, as mentioned earlier. The raised temperature has consequently led to grain growth [38]. According to Bhadeshia [39], B and LB form at a higher cooling rate than GBF and WF during the temperature transition from austenite during the welding process. The presence of B and LB in the double V-shaped groove welding is associated with an increased

welding cooling rate. Since double V-shaped groove welding has experienced lower welding interpasses than V-shaped groove welding, this led to a lower welding interpass temperature [32] and therefore an increased cooling rate [40]. A study by Peng et al. [41] on the Q550W weathering steel welding by GMAW showed that with the increased heat input, there is a microstructure transition in the acicular ferrite that changes from bainite acicular ferrite (B-AF) to Widmanstätten acicular ferrite (WF-AF).

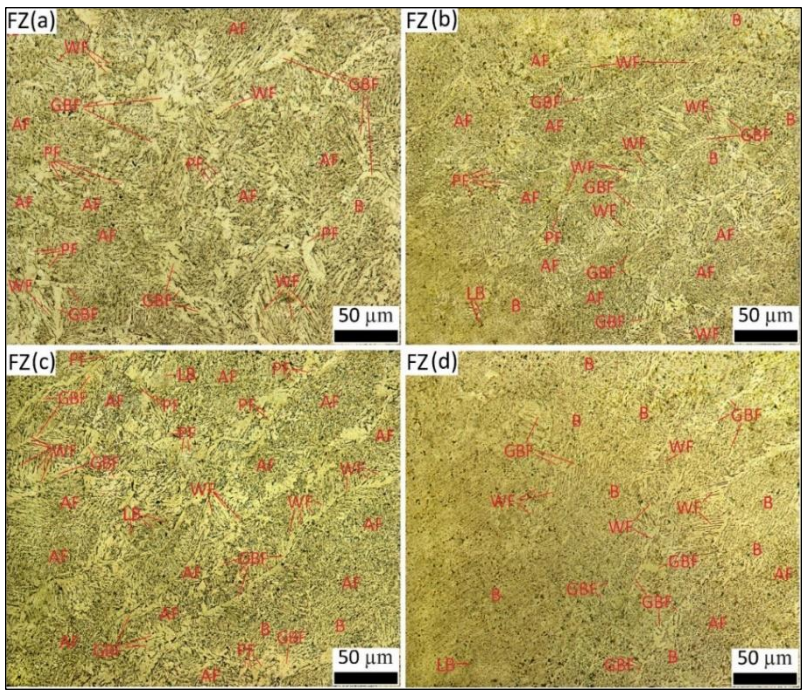

Figure 9: FZ microstructure magnified 20 times showing, (a) welding experiment 1, (b) welding experiment 2, (c) welding experiment 3, and (d) welding experiment 4

The FZ microstructure indicates that higher tensile strength was shown at microstructure with reduced GBF volume fraction; however, the FZ of welding experiment 3 (V-shaped groove welding), as seen in Figure 9(c), showed increased GBF volume fraction and higher tensile strength (251 MPa). It is suggested to be related to the welding interpass heat input due to the multiple passes that caused grain growth and therefore wider GBF. Nonetheless, it is important to relate to the behavior of HAZ microstructure since it's critical in determining the mechanical properties of welding [42]. Peng et al. [41] concluded that the tensile strength of steel welding has

decreased with increased heat input. According to the study, weak grain refinement and dislocations in the crystal structure are the causes. The FZ hardness also increased with the reduced GBF and the presence of B and LB volume fractions.

The HAZ optical microstructure, as illustrated in Figure 10, showed the presence of P, PF, WF, AF, and C. Figures 10(a) and 10(c) correspond to HAZ for V-shaped grooved welding made at welding speeds of 100 and 150 mm/min, respectively.

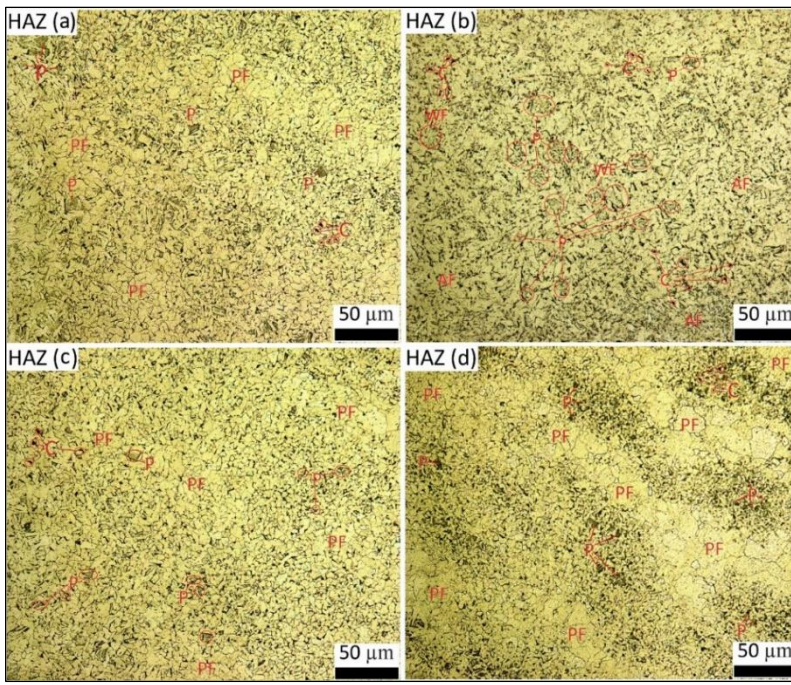

Figure 10: HAZ microstructure magnified 20 times showing, (a) welding experiment 1, (b) welding experiment 2, (c) welding experiment 3, and (d) welding experiment 4

Figure 10(c) shows finer perlitic and ferritic grains, which is related to the fact that the welding experiment was exposed to lower heat input. In contrast to welding experiment 1, as seen in Figure 10(a), which presented coarser grains. The HAZ has shown a coarser grain structure in Figure 10(b), which corresponds to welding experiment 2, which presented increased AF volume friction. In contrast to the increased PF and less diffusive P grain structure shown in Figure 10(d). The later, which corresponds to double V-shaped groove welding (welding experiment 4), showed the least change in

HAZ microstructure compared to the other samples (Figures 10(a), 10(b), and 10(c), taking into account the original microstructure of the base metal as shown in Figure 8. That is because the HAZ of welding experiment 4 (Figure 10(d)) was exposed to a lower heat input than welding experiment 2 (Figure 10(b)). However, the HAZ of V-shaped groove welding (Figures 10(a) and 10(c)) showed a much finer grain structure; it's suggested to be related to the increased interpass heat input that caused grain recrystallization or regrowth.

Higher welding tensile strengths (251 MPa and 228 MPa for welding experiments 3 and 4, respectively) and HAZ hardness (2629 NHN for welding experiment 4) were shown at HAZ with a finer ferritic and perlitic grain structure, as seen in Figures 10(c) and 10(d). However, the higher hardness in V-shaped groove welding is suggested to be associated with the finer grain structure, which promotes higher tensile strength.

Fracture numerical analysis

The kinematic boundary conditions are applied to the welding tensile test sample model for the V-shaped groove and the double V-shaped groove in Figure 11. The upper grip section is constrained for movement in all directions (U1=U2=U3=0), as seen in Figure 11. Although the lower grip was allowed to displace in the Z direction (U3). The meshing of the model is presented in Figure 12. After modeling, the unscaled deformed distances (Figures 13(c) and 14(c)) are 550 mm for the V-shaped groove and 700 mm for the double V-shaped groove, whereas the scaled deformed distance is 495 mm for both groove samples.

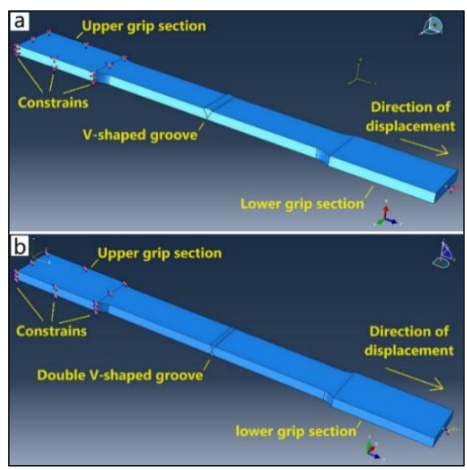

Figure 11: Kinematic boundary conditions showing constraints and direction of displacement of tensile test model sample for (a) V-shaped groove and (b) double V-shaped groove welding

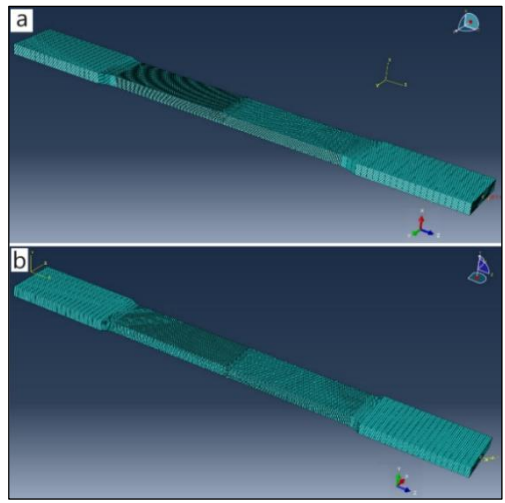

Figure 12: Meshing of tensile test model sample into hexahedral elements for (a) V-shaped groove and (b) double V-shaped groove welding

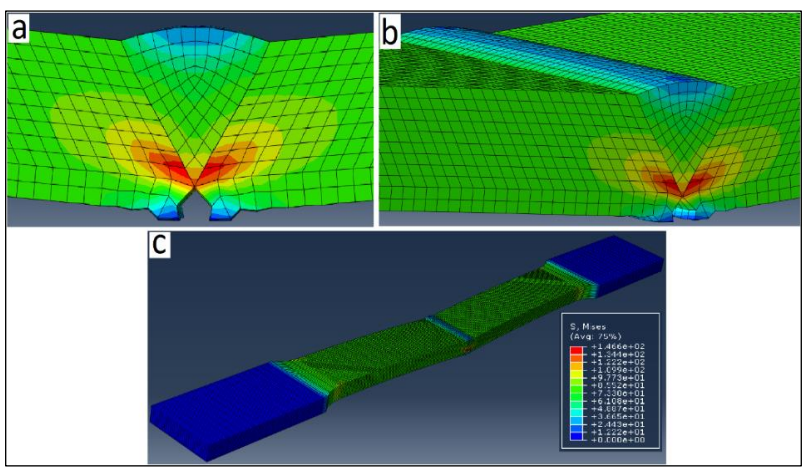

Figure 13: FE model for V-shaped groove welding during tensile test (a) 2D view of welding area, (b) 3D view of welding area, and (c) 3D view of welding sample

The Von Mises stress, also known as the "equivalent stress" is seen in Figure 13 and Figure 14, which is the measure of the overall stress in a material caused by multiple types of loading. The von Mises stress, also known as S. Mises is used to determine the maximum stress that a material can withstand

before failing. Figure 13 shows the FE model for V-shaped groove welding. Figures 13(a) and 13(b) illustrate the red concentration of higher stresses at the welding root at the bottom of the joint groove, which are caused by tensile forces. We suggest that these stresses are tensile because the bottom of the joint is the weakest point, as the welding root minimizes the FZ volume friction. It's considered the deformation is unbalanced and observe bending in the direction of the root fracture. The stresses on the top surface of welding are essentially compressed.

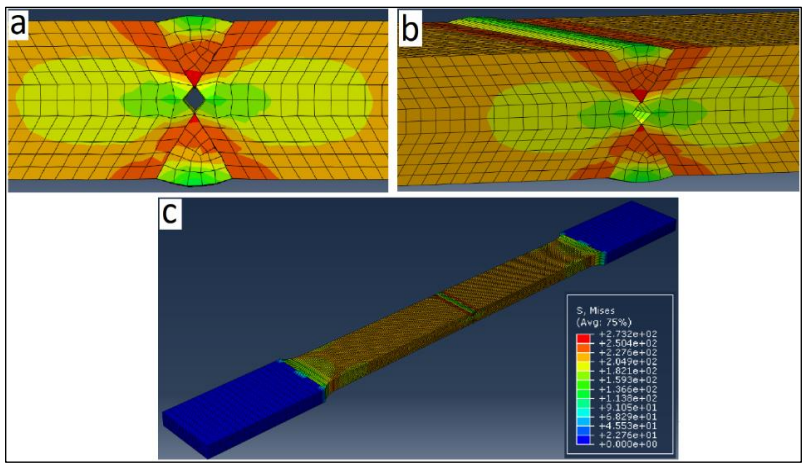

Figure 14: FE model for double V-shaped groove welding during tensile test (a) 2D view of welding area, (b) 3D view of welding area, and (c) 3D view of welding sample

Figure 14 illustrates the FE model for double V-shaped groove welding, which observes more balanced stresses on both sides of the groove. The model exhibits balanced deformation, with higher tensile stresses at the welding roots and around the top. From Figures 13 and 14, the welding roots showed that they experienced a higher tensile force, which indicates that higher tensile strength depends on a strong welding root that has a higher dilution. The models also show that when the tensile exceeds the yield point, the welding root begins to plasticize first since it has shown higher stresses, initiating the fracture process. Although S.Mises in Figure 14(c) shows that double V-shaped welding can handle higher stresses before failure (2.732e+02) than V-shaped welding (1.466e+02) as seen in Figure 13(c), which means theoretically it has higher tensile stress. However, the FEA only models the tensile test against the groove shape regardless of the welding hardness or the FZ and HAZ microstructure, or the welding dilution due to the welding heat

input or welding interpasses. All of these factors may affect welding's transverse tensile strength with respect to the groove shape.

Conclusions

GTAW welded mild steel grade S235JR at a variety of welding speeds and groove shapes. Higher welding traverse tensile strength was shown at higher welding speed and V-shaped groove welding. Higher FZ hardness was found to be associated with higher tensile strength. V-shaped groove welding has shown higher GBF and PF volume friction in the FZ and finer PF in the HAZ due to its higher interpass heat input. Higher traverse tensile strength welding has shown increased B and LB volume friction in FZ and finer perlitic and ferritic grain structure in HAZ. The FEA has concluded that failure of the welding due to transverse tensile starts at the welding root, and a double V-shaped groove has presented deformation balance compared to V-shaped groove welding during the tensile test.

Contributions of Authors

The author affirms that this work is an individual effort and has reviewed and approved its final version.

Funding

This work was solely supported by the author and has received no specific grant from any funding agency.

Conflict of Interests

The author declares no conflicts of interest.

Acknowledgment

The author would like to thank his family for their support and encouragement throughout this study. A sincere appreciation goes to the Libyan Iron and Steel Company for their help, and to the staff of the welding laboratory at Altaibat Food Inc. An appreciation goes to the College of Mechanical Engineering Technology, Benghazi.

References

[1] E. Korkmaz and C. Meran, "Mechanical properties and microstructure characterization of GTAW of micro-alloyed hot rolled ferritic XPF800 steel," *Engineering Science and Technology an International Journal*, vol. 24, no. 2, pp. 503-513, 2021. https://doi.org/10.1016/j.jestch.2020.04.006

[2] J. Luijan, P. Surin, and K. Eidhed, "The effect of welding parameters on joining dissimilar low carbon steel and 3cr12 ferritic stainless steel by GTAW with ER308L filler metal," in *IOP Conference Series: Journal of Physics*, vol. 1519, no. 1, p. 012010, 2020. https://doi.org/10.1088/1742-6596/1519/1/012010

[3] N. Sahu, B. K. Barik, S. Sahoo, S. K. Badjena, and S. K. Sahoo, "Studies on metallurgical and corrosion characteristics of dissimilar GTAW welding of alloy 800 and SS316L using multicomponent activated flux," *Materials Today: Proceedings*, vol. 44, pp. 2533-2536, 2021. https://doi.org/10.1016/j.matpr.2020.12.607

[4] C. S. Abima, S. A. Akinlabi, N. Madushele, O.S. Fatoba, and E. T. Akinlabi, "Experimental Investigation of TIG-welded AISI 1008 Carbon Steel," in *IOP Conference Series: Materials Science and Engineering*, vol. 1107, no. 1, p. 012036, 2021. https://doi.org/10.1088/1757-899x/1107/1/012036

[5] K. V. Satheesh Kumar, K. A. Srikishore, A. Shek Mohammed Asiq, and R. Sudharsan, "Experimental Investigation of Tensile Strength and Hardness in GMAW/GTAW Butt Welded Joints with Various Shielding Gas Compositions," in *Materials, Design, and Manufacturing for Sustainable Environment: Select Proceedings of ICMDMSE*, pp. 57-78, 2021. https://doi.org/10.1007/978-981-15-9809-8_5

[6] S. Sirohi, S. M. Pandey, A. Świerczyńska, G. Rogalski, N. Kumar, M. Landowski, and C. Pandey, "Microstructure and mechanical properties of combined GTAW and SMAW dissimilar welded joints between Inconel 718 and 304L austenitic stainless steel," *Metals*, vol. 13, no. 1, p. 14. 2022a. https://doi.org/10.3390/met13010014

[7] S. Sirohi, A. Kumar, S. Soni, G. Dak, S. Kumar, A. Świerczyńska, and C. Pandey, "Influence of PWHT parameters on the mechanical properties and microstructural behavior of multi-pass GTAW joints of P92 steel," *Materials*, vol. 15, no. 12, p. 4045, 2022b. https://doi.org/10.3390/ma15124045

[8] T. Rodríguez-Hernández, V. L. Cruz-Hernández, M. A. García-Rentería, R. Torres-Gonzalez, S. García-Villarreal, F. F. Curiel-López, and L. A. Falcón-Franco, "First assessment on the microstructure and mechanical properties of GTAW-GMAW hybrid welding of 6061-t6 AA," *Journal of Manufacturing Processes*, vol. 59, pp. 658-667, 2020. https://doi.org/10.1016/j.jmapro.2020.09.069

[9] K. Durgaprasad, S. Pal, and M. Das, "Metallurgical and mechanical properties evolution in cusp-magnetic field-assisted GTAW of low carbon steel," *Proceedings of the Institution of Mechanical Engineers, Part C: Journal of Mechanical Engineering Science, First online*, 2022. https://doi.org/10.1177/09544062221135520

[10] M. Jawad, M. Jahanzaib, M. A. Ali, M. U. Farooq, N. A. Mufti, C. I. Pruncu, and A. Wasim, "Revealing the microstructure and mechanical attributes of pre-heated conditions for gas tungsten arc welded AISI 1045 steel joints," *International Journal of Pressure Vessels and Piping*, vol. 192, p. 104440, 2021. https://doi.org/10.1016/j.ijpvp.2021.104440

[11] C. Chen, C. Fan, X. Cai, S. Lin, C. Yang, and Y. Zhuo, "Microstructure and mechanical properties of Q235 steel welded joint in pulsed and un-pulsed ultrasonic assisted gas tungsten arc welding," *Journal of Materials Processing Technology*, vol. 275, p. 116335, 2020. https://doi.org/10.1016/j.jmatprotec.2019.116335

[12] S. Mohanty, G. K. Mohanta, A. K. Senapati, and K. C. Rath, "Taguchi grey relational analysis for optimal process parameter of low carbon steel welded by GTAW by using ER309L filler material," *Materials Today: Proceedings*, vol. 44, pp. 2556-2561, 2021. https://doi.org/10.1016/j.matpr.2020.12.631

[13] Y. Dubey, P. Sharma, and M. P. Singh, "Experimental investigation for GTAW optimization using genetic algorithm on S-1 tool steel," *Materials Today: Proceedings*, 2023. https://doi.org/10.1016/j.matpr.2023.02.174

[14] S. Saidin, D. Andud, Y. H. Manurung, M. F. Mat, N. Nordin, and M. Leitner, "Effects of High Frequency Mechanical Impact on Fatigue Life of Semi-Automated Gas Metal Arc Welding (GTAW) of HSLA Butt Weld," in *MATEC Web of Conferences*, vol. 269, p. 06002, 2019. https://doi.org/10.1051/matecconf/201926906002

[15] G. İrsel, "Study of the microstructure and mechanical property relationships of shielded metal arc and TIG welded S235JR steel joints," *Materials Science and Engineering: A*, vol. 830, p. 142320, 2022. https://doi.org/10.1016/j.msea.2021.142320

[16] S. Elfallah, "Effect of GTAW on the tensile strength and hardness of mild steel," *Annals of "Dunarea de Jos" University of Galati. Fascicle XII, Welding Equipment and Technology*, vol. 33, pp. 95-100, 2022b. https://doi.org/10.35219/awet.2022.08

[17] M. Singh, A. S. Shahi, and D. Singh, "Effect of weld groove volume on the mechanical and metallurgical performance of GTA welded martensitic stainless steel (AISI 410 SS) joints," *Materials Today: Proceedings*, vol. 28, pp. 1580-1587, https://doi.org/10.1016/j.matpr.2020.04.844

[18] R. Kant, S. Pandey, R. Singh, and P. Tanwar, "Influence of process parameters on weld bead geometry and mechanical properties in

GTAW," *Trends in Manufacturing Processes: Select Proceedings of ICFTMM 2018*, pp. 111-117, 2020. https://doi.org/10.1007/97

[19] G. Dak, and C. Pandey, "Study on effect of weld groove geometry on mechanical behavior and residual stresses variation in dissimilar welds of P92/SS304L steel for USC boilers," *Archives of Civil and Mechanical Engineering*, vol. 22, no. 3, pp. 140, 2022. https://doi.org/10.1007/s43452-022-00468-8

[20] D. Pathak, R. P. Singh, S. Gaur, and V. Balu, "Influence of groove angle on hardness and reinforcement height of shielded metal arc welded joints for low carbon AISI 1016 steel plates," *Materials Today: Proceedings*, vol. 38, pp. 40-43, 2021. https://doi.org/10.1016/j.matpr.2020.05.597

[21] E. Çetkin, Y. H. Çelik, and Ş. Temiz, "Effect of welding parameters on microstructure and mechanical properties of AA7075/AA5182 alloys joined by TIG and MIG welding methods," *Journal of the Brazilian Society of Mechanical Sciences and Engineering*, vol. 42, pp. 1-12, 2020. https://doi.org/10.1007/s40430-019-2119-7

[22] ASTM, "Standard Hardness Conversion Tables for Metals Relationship Among Brinell Hardness, Vickers Hardness, Rockwell Hardness, Superficial Hardness, Knoop Hardness, Scleroscope Hardness, and Leeb Hardness," *ASTM E140-12B(2019)e1*, 2019. https://doi.org/10.1520/E0140-12BR19E01

[23] ASTM, "Standard test methods for tension testing of metallic materials," *E8/E8M-22*, 2024. https://doi.org/10.1520/E0008_E0008M-22

[24] S. Roy, B. Silwal, A. Nycz, M. Noakes, E. Cakmak, P. Nandwana, and Y. Yamamoto, "Investigating the effect of different shielding gas mixtures on microstructure and mechanical properties of 410 stainless steel fabricated via large scale additive manufacturing," *Additive Manufacturing*, vol. 38, p. 101821, 2021. https://doi.org/10.1016/j.addma.2020.101821

[25] J. R. Deepak, J. J. Jeevahan, D. Ramachandran, S. S. Suhas, and P. P. Reddy, "XRD investigation of GTAW, GMAW, LBW, and AGTAW Corten A588 grade steel weldments," *Materials Today: Proceedings*, vol. 47, pp. 4844-4851, 2021. https://doi.org/10.1016/j.matpr.2021.06.081

[26] D. Purnama, and H. Oktadinata, "Effect of shielding gas and filler metal to microstructure of dissimilar welded joint between austenitic stainless steel and low carbon steel," in *IOP Conference Series: Materials Science and Engineering*, vol. 547, no. 1, p. 012003, 2019. https://doi.org/10.1088/1757-899X/547/1/012003

[27] P. Murali, and R. Gopi, "Experimental investigation of tungsten inert gas welding (TIG) using Ar/Ar-CO_2 shielding gas on alloy steels," *Materials Today: Proceedings*, vol. 39, pp. 812-817, 2021. https://doi.org/10.1016/j.matpr.2020.09.776

[28] V. Bhanu, S. M. Pandey A. Gupta, and C. Pandey, "Dissimilar weldments of P91 and Incoloy 800HT: Microstructure, mechanical properties, and residual stresses," *International Journal of Pressure Vessels and Piping*, vol. 199, p. 104782, 2022. https://doi.org/10.1016/j.ijpvp.2022.104782

[29] I. Voiculescu, V. Geanta, E. V. Stefanescu, G. Simion, E. Scutelnicu, "Effect of Diffusion on Dissimilar Welded Joint between Al0.8CoCrFeNi High-Entropy Alloy and S235JR Structural Steel," *Metals***,** vol. 12, p. 548, 2022. https://doi.org/10.3390/met12040548

[30] A. K. Krella, D. E. Zakrzewska, and A. Marchewicz, "The resistance of S235JR steel to cavitation erosion," *Wear*, vol. 452-453, p. 203295, 2020. https://doi.org/10.1016/j.wear.2020.203295

[31] N. Kumar, P. Kumar, R. S. Vidyarthy, and C. Pandey, "Numerical and experimental investigation of autogenous GTAW weld between IN 718/ASS 304L," *International Journal on Interactive Design and Manufacturing (IJIDeM)*, vol. 18, pp. 1523-1538, 2024. https://doi.org/10.1007/s12008-024-01764-8

[32] R. Scharf-Wildenhain, A. Haelsig, J. Hensel, K. Wandtke, D. Schroepfer, A. Kromm, and T. Kannengiesser, "Influence of Heat Control on Properties and Residual Stresses of Additive-Welded High-Strength Steel Components," *Metals*, vol. 12, no. 6, p. 951, 2022. https://doi.org/10.3390/met12060951

[33] H. Ji, M. K. Gupta, Q. Song, W. Cai, T. Zheng, Y. Zhao, and D. Y. Pimenov, "Microstructure and Machinability Evaluation in Micro Milling of Selective Laser Melted Inconel 718 Alloy," *Journal of Materials Research and Technology*, vol. 14: pp. 348-362, 2021. https://doi.org/10.1016/j.jmrt.2021.06.081

[34] T. Lahtinen, P. Vilaça, P. Peura, and S. Mehtonen, "MAG welding tests of modern high strength steels with minimum yield strength of 700 MPa," *Applied Sciences*, vol. 9, no. 5, p. 1031, 2019. https://doi.org/10.1016/j.ijfatigue.2019.04.034

[35] N. Sridharan, J. Bunn, M. Kottman, C. M. Fancher, A. Payzant, M. Noakes, and S. S. Babu, "Consumable Development to Tailor Residual Stress in Parts Fabricated using Directed Energy Deposition Processes," *Additive Manufacturing*, vol. 39, p. 101837, 2021. https://doi.org/10.1016/j.addma.2021.101837

[36] M. Kowal, and M. Szala, "Diagnosis of the microstructural and mechanical properties of over century-old steel railway bridge components," *Engineering failure analysis*, vol. 110, p. 104447, 2020. https://doi.org/10.1016/j.engfailanal.2020.104447

[37] M. Pinson, S. M. Das, H. Springer, T. Depover, and K. Verbeken, "The addition of aluminum to brittle martensitic steels in order to increase ductility by forming a grain boundary ferritic microfilm," *Scripta*

Materialia, vol. 213, p. 114606, 2022. https://doi.org/10.1016/j.scriptamat.2022.114606

[38] P. Henckell, M. Gierth, Y. Ali, J. Reimann, and J. P. Bergmann, "Reduction of energy input in wire arc additive manufacturing (WAAM) with gas metal arc welding (GMAW)," *Materials*, vol. 13, no. 11, p. 2491, 2020. https://doi.org/10.3390/ma13112491

[39] H. K. D. H. Bhadeshia. Bainite in Steels, Eds: Yang, Z. and Zhang, F. 3rd Ed. CRC Press, 2020.

[40] J. Li, H. Li, Y. Liang, P. Liu, and L. Yang, "The microstructure and mechanical properties of multi-strand, composite welding-wire welded joints of high nitrogen austenitic stainless steel," *Materials*, vol. 12, no. 18, p. 2944, 2019. https://doi.org/10.3390/ma12182944

[41] T. Peng, C. Fu, Z. Qin, B. He, X. Hu, T. Zhu, and Y. Liu, "Microstructural characterization and mechanical properties of a Q550W weathering steel welded joint under different heat inputs," *Journal of Materials Science*, vol. 57, no. 34, pp. 16528-16540, 2022. https://doi.org/10.1007/s10853-022-07688-6

[42] V. García-García, I. Mejía, F. Reyes-Calderón, J. A. Benito, and J. M. Cabrera, "FE thermo-mechanical simulation of welding residual stresses and distortion in Ti-containing TWIP steel through GTAW process," *Journal of Manufacturing Processes*, vol. 59, pp. 801-815, 2020. https://doi.org/j.jmapro.2020.09.042